applied sciences

MDPI

Article

Research on Propagation Characteristics of Tire Cavity Resonance Noise in the Automobile Suspension

Xiaojun Hu [1,*], Xiandong Liu [2,*], Yingchun Shan [2] and Tian He [2]

[1] School of Mechanical, Electronic and Control Engineering, Beijing Jiaotong University, Beijing 100044, China
[2] School of Transportation Science and Engineering, Beihang University, Beijing 100191, China; shanych@buaa.edu.cn (Y.S.); hetian@buaa.edu.cn (T.H.)
* Correspondence: xjhu@bjtu.edu.cn (X.H.); liuxiandong@buaa.edu.cn (X.L.)

Featured Application: The research of propagation characteristics can provide a significance and value for McPherson suspension system design.

Abstract: Tire cavity resonance noise (TCRN) is one of main contributors to vehicle interior noise, which has long been a concern in the automotive industry and academia. As suspension is crucial for the propagation of TCRN energy into the vehicle, the propagation characteristics of energy in automobile suspension is studied in this research. Firstly, the finite element model of a McPherson suspension system connected to an aluminum alloy wheel with a Y-shaped spoke was established. Then, a modal analysis and response calculations of the McPherson suspension system connected to the aluminum alloy wheel with a Y-shaped spoke were carried out. Finally, the propagation characteristics of TCRN in the McPherson suspension system connected to the aluminum alloy wheel with a Y-shaped spoke were studied and analyzed by the power flow method under different working conditions. The power flow output via the lower arm front bushing was the largest, while the output via the rear bushing was the smallest in the Y-spoke aluminum alloy wheel and suspension system. The areas in the suspension system with high stress are located at the steering knuckle, lower swing arm, and shock absorber. Therefore, study of the propagation characteristics can provide a basis for a McPherson suspension system design.

Keywords: tire cavity resonance noise; power flow method; McPherson suspension system; structural sound intensity; modal analysis

check for updates

Citation: Hu, X.; Liu, X.; Shan, Y.; He, T. Research on Propagation Characteristics of Tire Cavity Resonance Noise in the Automobile Suspension. *Appl. Sci.* **2023**, *13*, 12113. https://doi.org/10.3390/app132212113

Academic Editor: Edoardo Piana

Received: 11 August 2023
Revised: 31 October 2023
Accepted: 2 November 2023
Published: 7 November 2023

Copyright: © 2023 by the authors. Licensee MDPI, Basel, Switzerland. This article is an open access article distributed under the terms and conditions of the Creative Commons Attribution (CC BY) license (https://creativecommons.org/licenses/by/4.0/).

1. Introduction

With growing requirements for comfort in vehicles, TCRN has attracted the attention of researchers and has become an important area of tire–noise research around the world in recent years [1,2]. Although many results related to research on TCRN have been published, research of the propagation characteristics is still ongoing, and there is still no simple and easier method to suppress TCRN which could guide the design of automobiles [3,4].

The energy of TCRN propagates in the wheel and suspension system; an appropriate method must be chosen to reduce the propagation of energy in the wheel and suspension system. The power flow method is a widely applicable method to clarify the propagation characteristics of an elastic wave. In 1962, the power flow method was first put forward [5]. It was used to study the energy transfer to the seat through a vibration isolator, and a method was proposed to calculate the power flow of a structure [6]. The power flow method was used to compute the energy transfer of a thin-walled structure and to calculate power flow in simple two-dimensional structures [7]. Related research on surface energy and surface effects has proven to be helpful in power flow research [8–10]. The method of combining finite element analysis and vibration power flow calculations was used to obtain complex elastic foundation modal information using finite element software and to

substitute it into the elastic foundation admittance [11]. The power flow of the structural sound intensity method was introduced to study the propagation law of vibration energy in a thin-walled rectangular beam, and the difference in power flow at response points before and after applying a concentrated mass was examined [12]. Based on our power flow analysis, a power flow vibration and shock-fusion controller was proposed. This fusion controller covered the vibration control module that attenuated vibration excitation and the shock control module that buffered shock excitation and vibration [13]. The theory of vibration power flow was used to optimize the selection of the damping element bushing. The dynamic response of the system before and after parameter optimization and the influence of the bushing parameters on the power transmission were discussed in ref. [14].

The above works show that the power flow method has wide and mature applications in many fields, but so far, it has not been applied to research on the propagation characteristics of TCRN in a McPherson suspension system connected to an aluminum alloy wheel. Therefore, we applied the power flow method to research the propagation characteristics of TCRN in a McPherson suspension system connected to an aluminum alloy wheel. The laws of propagation characteristics of TCRN in a McPherson suspension system under different working conditions (loads, inflation pressures, or speeds) can provide the necessary basis for the design of a McPherson suspension system.

To this end, a finite element model of a McPherson suspension system connected to an aluminum alloy wheel was established, and modal analyses and response calculations of the McPherson suspension system were carried out. Finally, the power flow method was used to research the propagation characteristics of TCRN in a McPherson suspension system connected to an aluminum alloy wheel with a Y-shaped spoke, and the propagation characteristics of TCRN in the McPherson suspension system under different working conditions were obtained.

2. An Introduction to the Power Flow Method

To research the propagation of vibration energy in a structure, the power flow method is widely used. With it, the transmission path of the vibration energy in a structure can be identified [15]. Vibration power flow describes the energy consumption of structural vibrations or the ability of an external force to do work per unit time. The average vibration power flow in a period is generally used as a reference, and input power flow p in a structure is determined as follows:

$$p(t) = F(t)V(t) \tag{1}$$

where *F(t)* is the external force acting somewhere in the structure and *V(t)* is the velocity at that location produced by *F(t)*.

Average vibration power flow P corresponding to a certain period T is calculated as follows:

$$P = \frac{1}{T}\int_0^T F(t)V(t)dt \tag{2}$$

To calculate the power flow in a structure based on the finite element method, the nodal force and velocity vectors need to be calculated. The power flow per unit area of a certain section of the structure is its structural sound intensity, so stress can be introduced into the calculation. For an elastic body, the stress state at any point inside it can be expressed with six stress components: shear stress, i.e., τ_{xy}, τ_{yz}, and τ_{zx}, and normal stress, i.e., σ_x, σ_y, and σ_z. As an example, the stress distribution of a micro-element is shown in Figure 1.

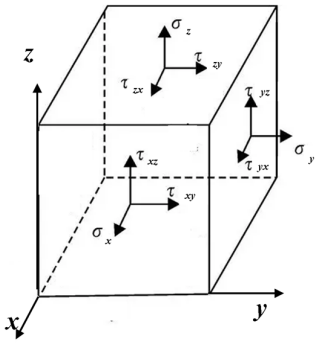


Figure 1. Micro-stress distribution.

The formula of structure sound intensity p_n is as follows:

$$p_n = -\frac{1}{2} Re(\tau_{n1} v_1^* + \tau_{n2} v_2^* + \sigma_n v_n^*) \tag{3}$$

where τ_{n1} and τ_{n2} are the shear stress in the 1-direction and 2-direction, respectively, σ_n is the normal stress in the normal n-direction, and v_1^*, v_2^*, and v_n^* are the velocity complex conjugates in the 1-direction, 2-direction, and n-direction, respectively.

It can be seen from the literature [16] that stress and displacement can be evaluated by calculating the harmonic response results. A solid element has three directions, x, y, and z, so the structural sound intensity in each direction is expressed as:

$$p_x = -\frac{\omega}{2} I_m \left(\tau_{xy} u_y^* + \tau_{xz} u_z^* + \sigma_x u_x^* \right) \tag{4}$$

$$p_y = -\frac{\omega}{2} I_m \left(\tau_{yx} u_x^* + \tau_{yz} u_z^* + \sigma_y u_y^* \right) \tag{5}$$

$$p_z = -\frac{\omega}{2} I_m \left(\tau_{zx} u_x^* + \tau_{zy} u_y^* + \sigma_z u_z^* \right) \tag{6}$$

where ω is the angular velocity, τ_{xy}, τ_{xz}, τ_{yx}, τ_{yz}, τ_{zx}, and τ_{zy} are the shear stress in the x, y, and z directions, respectively, u_x^*, u_y^*, and u_z^* are the displacement conjugates of the node in the x, y, and z directions, respectively, and p_x, p_y, and p_z are the structural sound intensity in the x, y, and z directions, respectively.

3. Establishment and Response Calculation of a McPherson Suspension System Model

3.1. Estabalishment of a McPherson Suspension System Connected to an Aluminum Alloy Wheel

The McPherson suspension system has a simple structure, low cost, and good performance, so it is widely used in the front suspension of automobiles. It consists of a coil spring, knuckle assembly, lower transverse arm, shock absorber, etc. With reasonable simplification, a McPherson suspension system model is shown in Figure 2a. With a connected 15-inch Y-spoke aluminum alloy wheel, the system model is shown in Figure 2b.

According to a tire cavity sound pressure distribution under the condition of 4000 N load, 0.22 MPa inflation pressure, and 60 km/h speed, the excitation acting on the rim is as shown in Figure 3, as described in previous literature [17,18]. The resonant sound pressure distribution function of the tire cavity is shown in Equation (7).

$$P(\theta, t) = (80 - 30\cos\theta + 30\sin\theta + 32\cos 2\theta - 24\sin 2\theta + 3\cos 3\theta + 14\sin 3\theta)\cos(2\pi f t) \tag{7}$$

where θ is the included angle between the radius of a certain point of the wheel rim and the radius of the contact position between the tire and the drum, and f is the tire cavity resonance frequency.

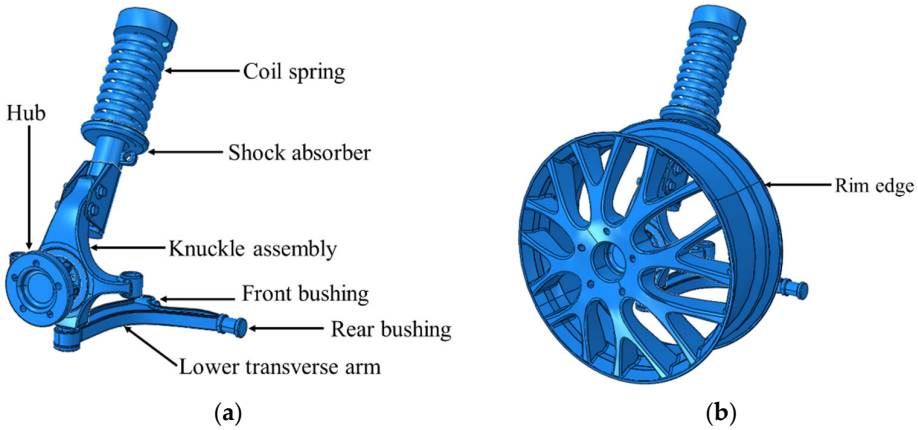


Figure 2. McPherson suspension system model. (**a**) McPherson suspension system. (**b**) Aluminum alloy wheel and McPherson suspension system.

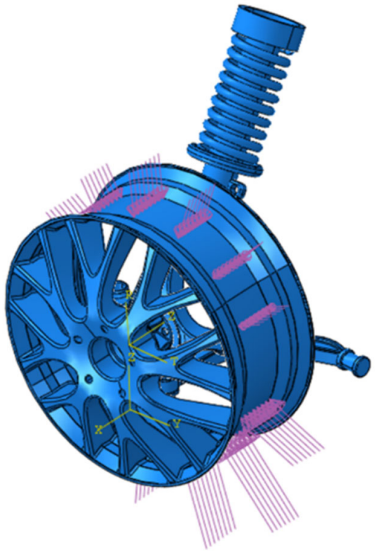
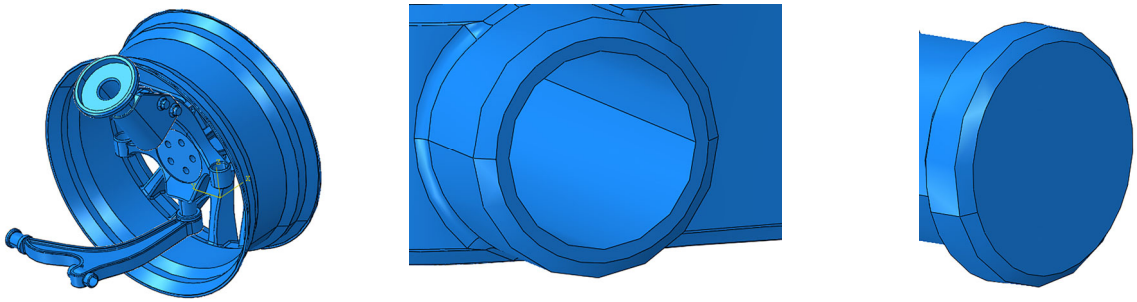


Figure 3. Load state of a McPherson suspension system.

For our simulation, some parts of the McPherson suspension system were simplified. For example, the outer end of the lower transverse arm was in bound contact with the knuckle assembly, and the inner end of the lower transverse arm was connected to the subframe through a bushing. The upper end of the shock absorber was fixed, and a spring unit was used to simulate the stiffness of the coil spring and the damping of the shock absorber. The spring unit was connected to the knuckle assembly through a cylindrical joint and to the upper end of the shock absorber at the other end. The knuckle assembly was in bound contact with the hub, and there was also bound contact between the hub and the aluminum alloy wheel. The stiffness and damping [19–23] of the associated bushings and spring units are shown in Table 1, and the simplified McPherson suspension system and transverse arm bushings are shown in Figure 4. A point was selected at the center of the bushing, and the bushing was linked to that point, with the connection between this point and the bushing representing the stiffness and damping. The input surface of the TCRN is the wheel rim surface. The output surface is the inner surface of the cylindrical joint support and the front and rear bushing surfaces of the lower transverse arm.

Table 1. Stiffness and damping of the bushing and spring unit.

Location	Direction	Stiffness (N/Mm)	Damping (N·s/mm)
Shock absorber upper end	X	10,000	1.5
	Y	10,000	
	Z	10,000	
Spring and shock absorber		25	1
Lower transverse arm front bushing	X	10,000	2
	Y	10,000	
	Z	1000	
Lower transverse arm rear bushing	X	500	0.8
	Y	500	
	Z	100	



(**a**) (**b**) (**c**)

Figure 4. Simplified McPherson suspension system and transverse arm bushings. (**a**) Simplified McPherson suspension. (**b**) Transverse arm front bushing. (**c**) Transverse arm rear bushing.

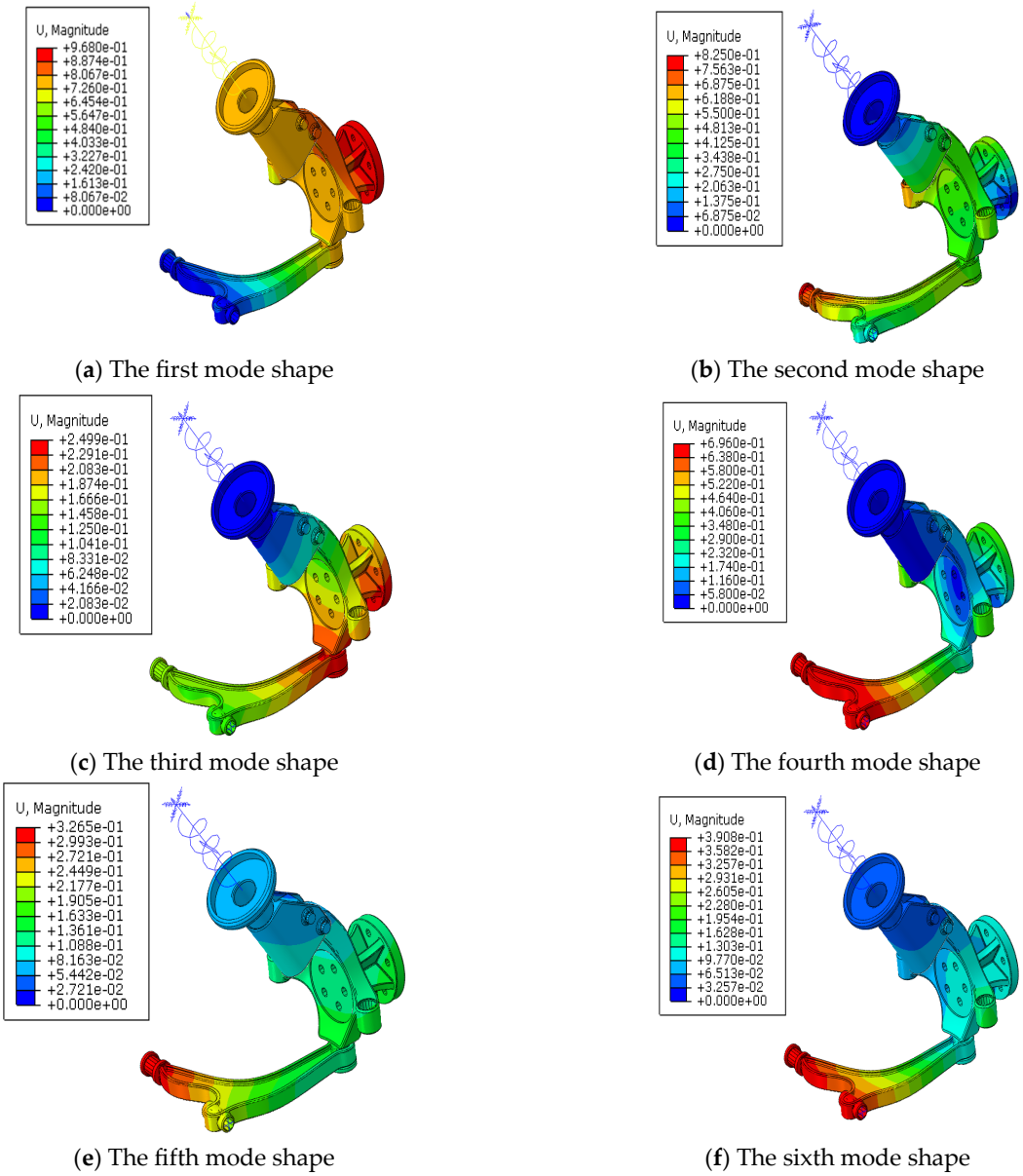
3.2. Modal Analysis and Response Calculation of a McPherson Suspension System

As a key link of TCRN propagation to the vehicle, the natural frequency of a suspension system is close to the tire cavity resonance frequency, which directly affects the propagation of this noise energy. We performed a modal analysis of a suspension system model using the Lanczos method in Abaqus 6.14. We focused only on a low-order modal analysis in the vast majority of cases and generally selected the first six orders of modes. Then, the first six orders of natural frequencies and vibration modes of the suspension system were taken, as shown in Figure 5. The finite element type was C3D10HS, which is a 10-node, general purpose quadratic tetrahedron with improved surface stress visualization. The DOF of C3D10HS is ten, and the behavior of the element type is in the form of a Lagrange description. The number of elements was 393,719.

It can be concluded that the steering knuckle bends in the longitudinal plane from the third order to the fourth order, and the lower swing arm bends in the longitudinal plane from the first to the sixth order. The natural frequencies of the suspension system are shown in Table 2. It can be seen that the sixth natural frequency was close to the resonance frequency of the tire cavity [17]. So, the FE suspension results were verified.

Table 2. Natural frequency of suspension system in each order.

Order	First	Second	Third	Fourth	Fifth	Sixth
Frequency (Hz)	28.44	60.30	81.56	131.62	201.82	245.92



(**a**) The first mode shape (**b**) The second mode shape

(**c**) The third mode shape (**d**) The fourth mode shape

(**e**) The fifth mode shape (**f**) The sixth mode shape

Figure 5. The first six orders of vibration mode shapes of the suspension system.

The Y-spoke aluminum alloy wheel and suspension system were simulated and analyzed. The suspension was made of steel and the type of elastic was isotropic. Our analysis was linear, using the implicit direct method of integration, where the steady state response of the system was calculated by directly integrating the original equations of the model. The dynamic response of tire cavity resonance noise was calculated, and the propagation characteristics of tire cavity resonance noise in suspension were obtained, providing a basis for the suppression of this noise. In our direct steady-state dynamics analysis of the suspension system, the response at the first frequency of tire cavity resonance was relevant. The defined sweep frequency range was 210–260 Hz, and 101 frequency points were defined, with one frequency excitation point every 0.5 Hz. Using this method, the stress and strain of the suspension system at the first natural frequency of the tire cavity resonance noise (238 Hz) were evaluated. The frequency (238 Hz) came from an experiment described in the literature [17], i.e., this value was not the result of other simulations. The stress and strain contours of the suspension system, obtained in the frequency domain, are shown in Figure 6. The unit of stress is MPa.

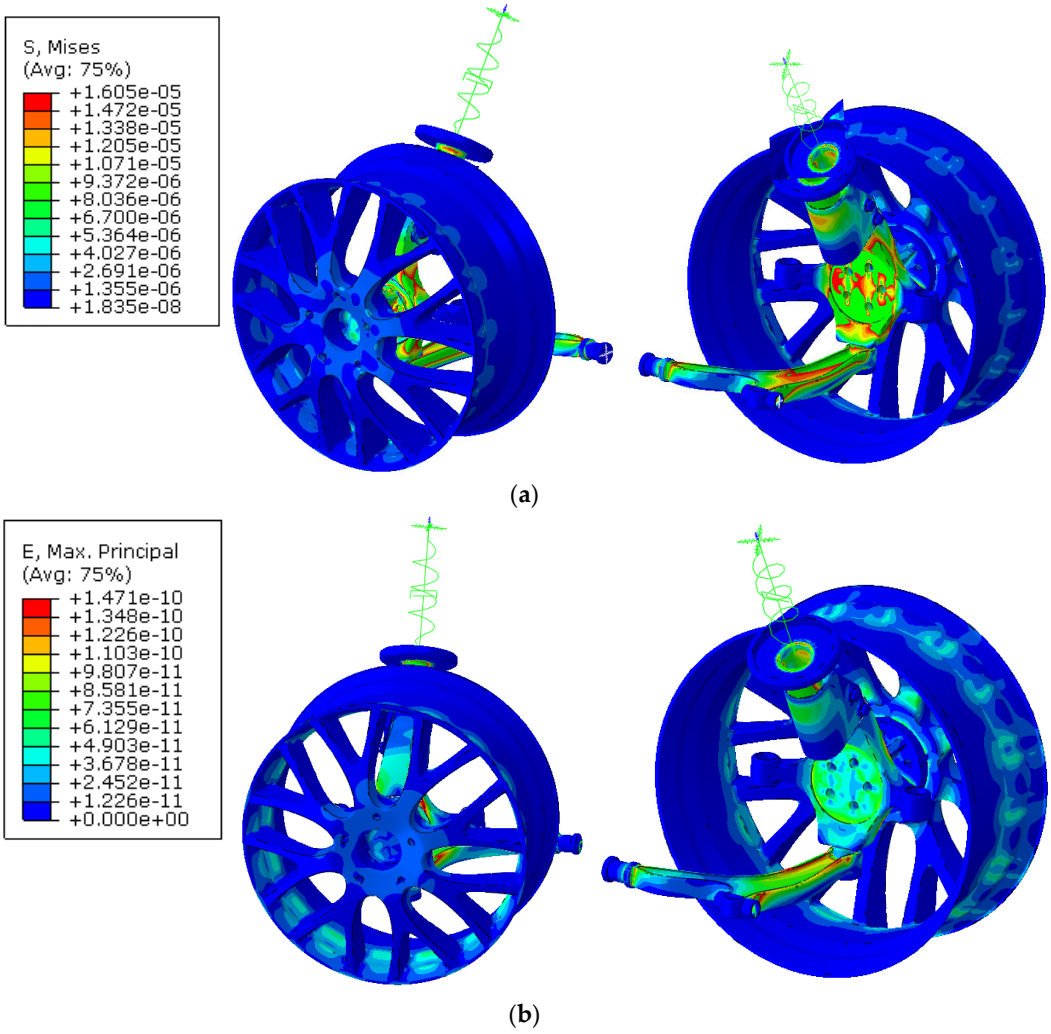


Figure 6. Stress and strain contour of a suspension system. (**a**) Stress contour of a suspension system. (**b**) Strain contour of a suspension system.

It can be seen from Figure 6 that the stress and strain of the suspension system were relatively large at the lower swing arm, steering knuckle, and shock absorber. Therefore, it can be speculated that the energy of the tire cavity resonance noise propagating to this area would also be large.

4. Power Flow Analysis of Tire Cavity Resonance Noise Propagation in a Suspension System

According to the steps of calculating the power flow in the wheel [18], the Y-spoke aluminum alloy wheel and suspension system were simulated. The distribution of structural sound intensity in the system under the conditions of 4000 N load, 0.22 MPa inflation pressure, and 60 km/h speed could be obtained, as shown in Figure 7. It can be seen that there was a large degree of structural sound intensity at the local spokes.

After the suspension system with a wheel had been studied, the real and imaginary values of stress and displacement at each point, the excitation frequency of the system response, and the point set data of the input and output surfaces were derived. The above txt format data were read by MATLAB R2014a, and the structural stress at each point in the wheel and the structural sound intensity of the input and output surfaces could be calculated according to the structural sound intensity formula. After obtaining the structural sound intensity and power flow, a vector diagram could be obtained by further programming. The contour of the structural sound intensity could be imported into the

simulation software through a program compiled in the Python language to realize the secondary development. Then, the contour of the structural sound intensity could be obtained. According to the steps described in ref. [18], the structural sound intensity vector distribution figures and a partial enlargement system in different planes could be obtained, as shown in Figure 8.

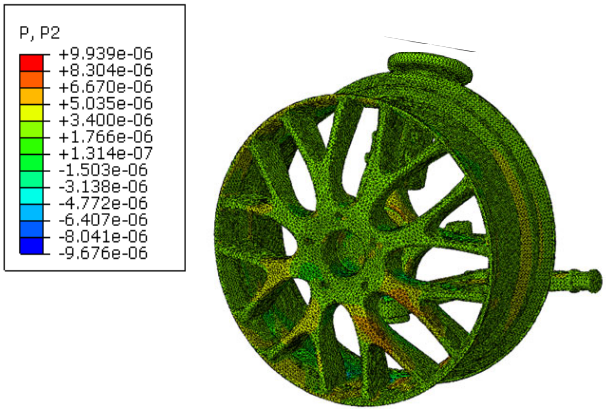


Figure 7. Power flow contour of aluminum alloy wheel and suspension system.

As shown in Figure 8, the structural sound intensity distribution of the suspension system was uneven. In the partial enlargement of Figure 8, the length of the arrows represents the amplitude of structural sound intensity, and the direction of the arrows represents the direction of structural sound intensity. During the transmission of structural sound intensity vectors, structural sound intensities of different directions and sizes meet and merge into a whole vector toward the hub center. Structural sound intensity vectors with the same frequency and different phases propagate from the spokes to the hub and continuously converge and dissipate.

For the Y-spoke aluminum alloy wheel and suspension system, data such as the sum of structural sound intensity and cross-sectional area at each point of the wheel input surface and output surface could be calculated. The power flow could be determined by formulas presented in ref. [18], and the results are shown in Table 3. Power flow is the product of the average structural sound intensity at the node and the corresponding cross-sectional area, as shown in Equation (8).

$$P_f = \frac{\sum p_{si}}{N} S \tag{8}$$

where P_f is the power flow of cross-section S, p_{si} is the structural sound intensity of point i, S is the area of the corresponding section, and N is the number of points.

The first output, second output, and third output in the table are the inner surface of the cylindrical auxiliary support and the front and rear bushing surfaces of the lower swing arm, respectively.

Table 3. Finite element calculation results of input and output sectional power flow.

Load Condition		Sum of Structural Sound Intensity (10^{-3} W/mm^2)	Number of Points	Cross Sectional Area (mm^2)	Power Flow of Cross Section (10^{-3} W)
4000 N	Input	2.897×10^{-2}	15,064	81,367	1.565×10^{-1}
	First output	1.068×10^{-4}	1840	7031	4.081×10^{-4}
	Second output	1.153×10^{-4}	462	2797	6.980×10^{-4}
	Third output	1.808×10^{-5}	350	1352	0.698×10^{-4}

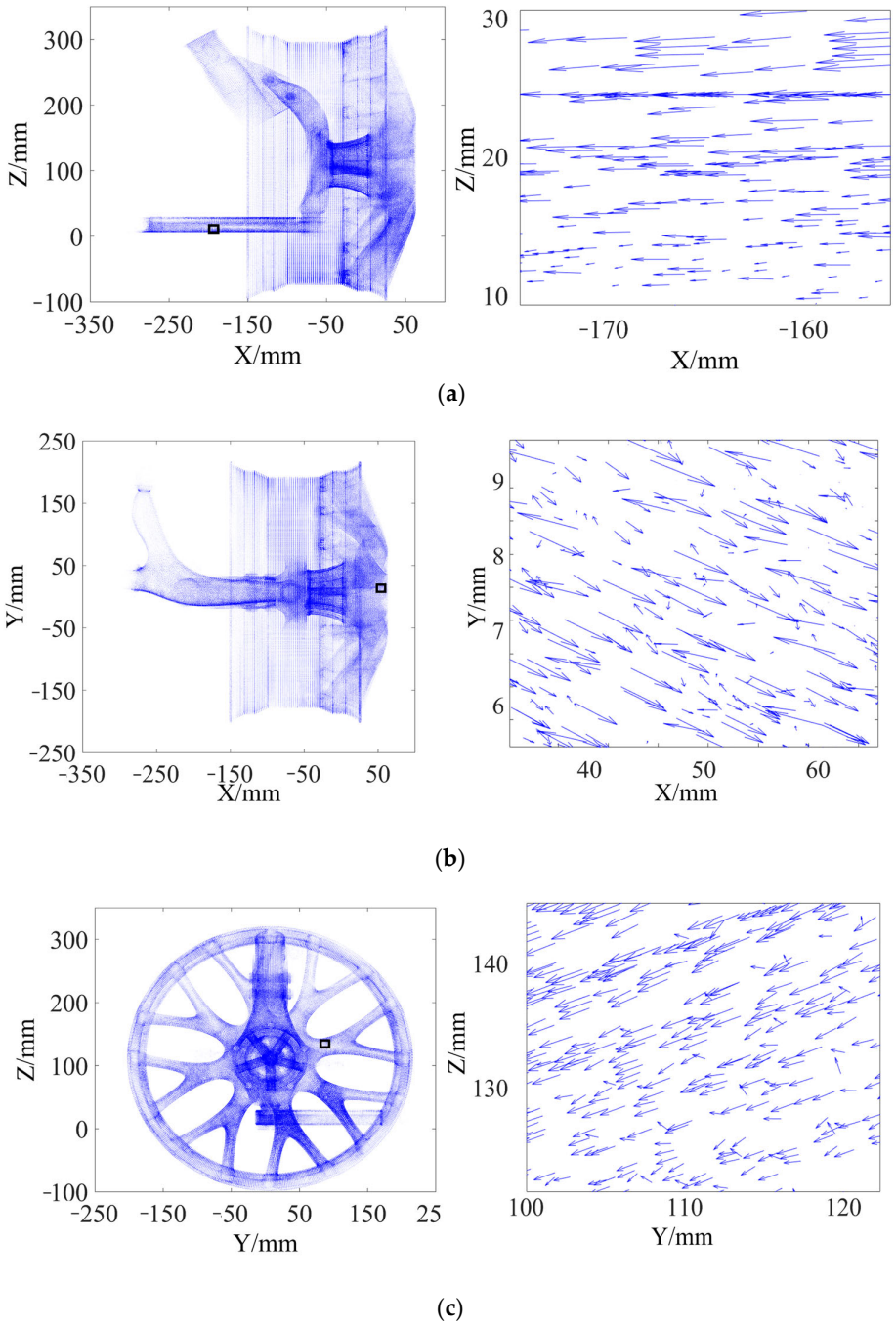


Figure 8. Distribution of the sound intensity vector of a suspension system in different planes and with partial enlargement. (**a**) XZ plane sound intensity vector distribution diagram and partial enlargement. (**b**) XY plane sound intensity vector distribution diagram and partial enlargement. (**c**) YZ plane sound intensity vector distribution diagram and partial enlargement.

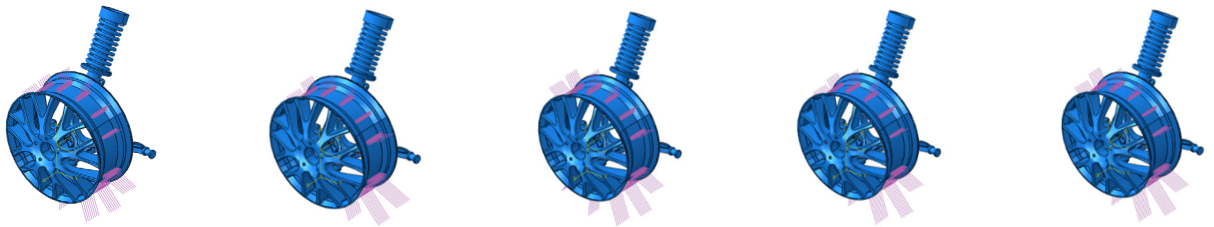
It can be seen from Table 3 that for the suspension system under 4000 N load, the output power flow of the front bushing of the lower swing arm was the largest and that of the rear bushing was the smallest. Therefore, special attention should be paid to the front bushing of the lower swing arm in order to suppress the transmission of the resonant noise energy of the tire cavity into the vehicle.

For different vehicle speeds and load conditions, the sound pressure amplitude function of the tire cavity resonance noise experienced by the wheels is shown in Table 4.

Table 4. Sound pressure amplitude function of wheels under various working conditions.

Tire Working Condition		Sound Pressure Amplitude Function
0.22 MPa 60 km/h	2500 N	$P(\theta,t) = (43 - 18\cos\theta + 19\sin\theta + 12\cos 2\theta - 5\sin 2\theta - \cos 3\theta - 4\sin 3\theta)\cos(2\pi ft)$
	3000 N	$P(\theta,t) = (55 - 9\cos\theta + 45\sin\theta - 2\cos 2\theta - 27\sin 2\theta + 8\cos 3\theta + \sin 3\theta)\cos(2\pi ft)$
	3500 N	$P(\theta,t) = (88 - 34\cos\theta + 6\sin\theta + 18\cos 2\theta - 6\sin 2\theta)\cos(2\pi ft)$
	4000 N	$P(\theta,t) = (80 - 30\cos\theta + 30\sin\theta + 32\cos 2\theta - 24\sin 2\theta + 3\cos 3\theta + 14\sin 3\theta)\cos(2\pi ft)$
	4500 N	$P(\theta,t) = (92 - 37\cos\theta + 34\sin\theta + 29\cos 2\theta - 35\sin 2\theta)\cos(2\pi ft)$
3500 N 50 km/h	0.16 MPa	$P(\theta,t) = (33 - 8\cos\theta + 7\sin\theta + 13\cos 2\theta - 11\sin 2\theta + \cos 3\theta + 6\sin 3\theta)\cos(2\pi ft)$
	0.19 MPa	$P(\theta,t) = (53 - 11\cos\theta + 7\sin\theta + 5\cos 2\theta - 11\sin 2\theta + \cos 3\theta - 6\sin 3\theta)\cos(2\pi ft)$
	0.22 MPa	$P(\theta,t) = (49 - 20\cos\theta + 6\sin\theta + 8\cos 2\theta - 8\sin 2\theta)\cos(2\pi ft)$
	0.25 MPa	$P(\theta,t) = (39 - \cos\theta + 11\sin\theta + 12\cos 2\theta - 14\sin 2\theta - 0.1\cos 3\theta + 7\sin 3\theta)\cos(2\pi ft)$
	0.28 MPa	$P(\theta,t) = (45 - 12\cos\theta + 5\sin\theta + 9\cos 2\theta - 11\sin 2\theta - \cos 3\theta - 5\sin 3\theta)\cos(2\pi ft)$
0.22 MPa 3000 N	20 km/h	$P(\theta,t) = (28 + 5\cos\theta + 11\sin\theta + 2\cos 2\theta - 12\sin 2\theta)\cos(2\pi ft)$
	30 km/h	$P(\theta,t) = (39 + 2\cos\theta + 12\sin\theta + 3\cos 2\theta - 13\sin 2\theta)\cos(2\pi ft)$
	40 km/h	$P(\theta,t) = (48 + \cos\theta + 13\sin\theta + 2\cos 2\theta - 12\sin 2\theta)\cos(2\pi ft)$
	50 km/h	$P(\theta,t) = (48 - 9\cos\theta + 14\sin\theta + 2\cos 2\theta - 10\sin 2\theta)\cos(2\pi ft)$
	60 km/h	$P(\theta,t) = (55 - 9\cos\theta + 45\sin\theta - 2\cos 2\theta - 27\sin 2\theta + 8\cos 3\theta + \sin 3\theta)\cos(2\pi ft)$

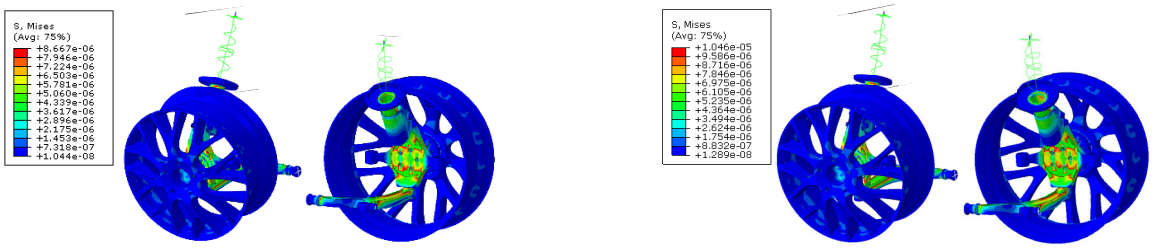
According to the amplitude distribution of resonant sound pressure in the tire cavity under different load conditions at 0.22 MPa inflation pressure and 60 km/h speed, as shown in Table 4 (the meanings of symbols in the function are the same as before), the model of a Y-spoke aluminum alloy wheel and suspension system after loading is shown in Figure 9.



(**a**) 2500 N load (**b**) 3000 N load (**c**) 3500 N load (**d**) 4000 N load (**e**) 4500 N load

Figure 9. Loading state of a suspension system under different loads.

The above five suspension system models under different loads were analyzed using the finite element method, and the response of an aluminum alloy wheel under the action of tire cavity resonance noise was calculated. The stress contour of the aluminum alloy wheel and suspension system under different loads is shown in Figure 10, and the corresponding strain contour is shown in Figure 11. The unit of stress is MPa.



(**a**) (**b**)

Figure 10. *Cont.*

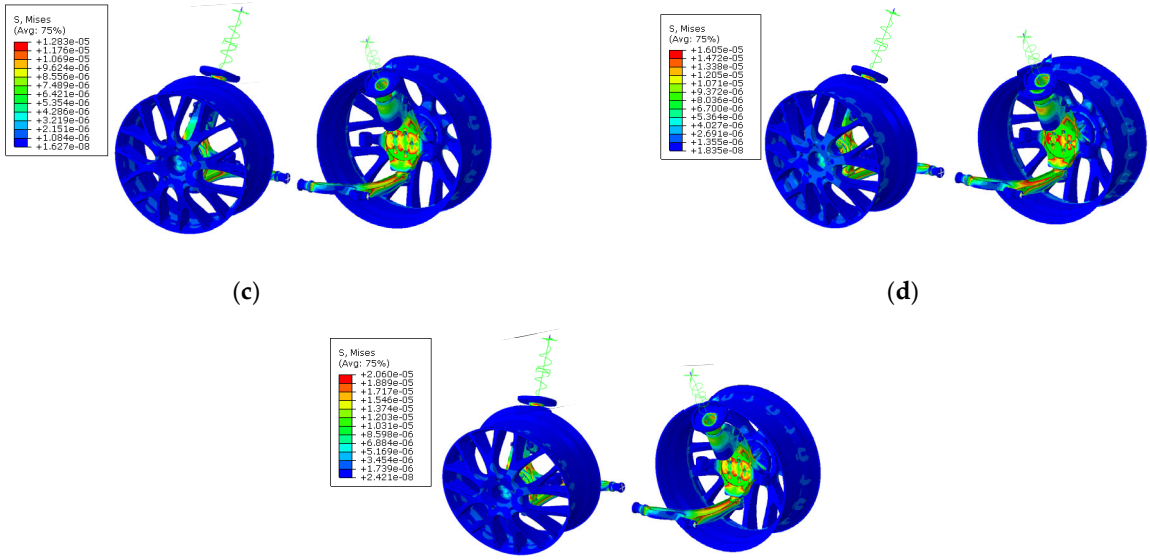


Figure 10. Stress contour of a suspension system under different loads. (**a**) Stress contour under 2500 N load. (**b**) Stress contouar under 3000 N load. (**c**) Stress contour under 3500 N load. (**d**) Stress contour under 4000 N load. (**e**) Stress contour under 4500 N load.

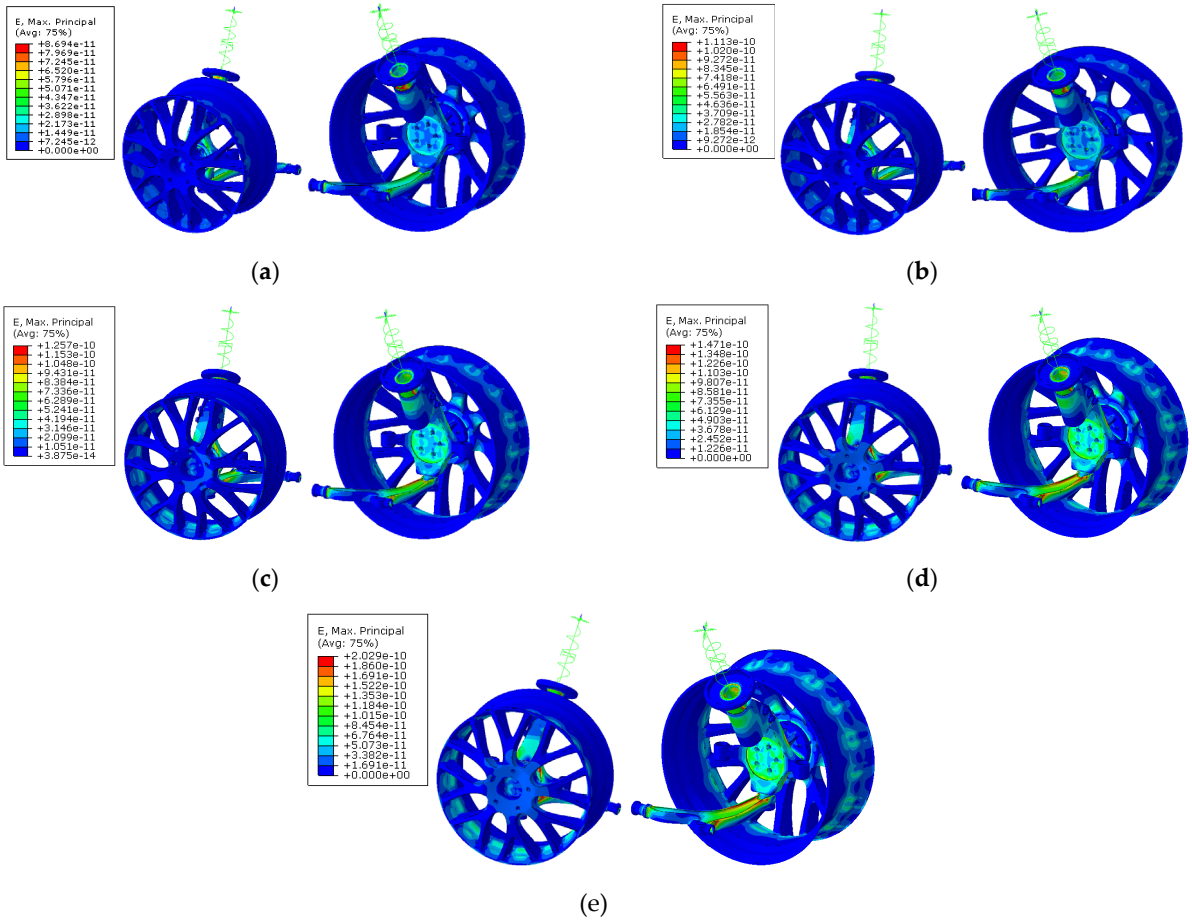


Figure 11. Strain contour of a suspension system under different loads. (**a**) Strain contour under 2500 N load. (**b**) Strain contour under 3000 N load. (**c**) Strain contour under 3500 N load. (**d**) Strain contour under 4000 N load. (**e**) Strain contour under 4500 N load.

It can be seen from the stress and strain contour of the suspension system under the above five different load conditions that the areas with high stress are located at the steering knuckle, lower swing arm, and shock absorber. The resonance noise energy of the tire cavity acted behind the rim, spread to the inside of the wheel, and finally spread to the steering knuckle, lower swing arm, and shock absorber through the spokes, resulting in high stress and strain in these three places. Therefore, it can be concluded that the energy transmitted to this area was concentrated, and the structural sound intensity was correspondingly large. With an increase of load, the stress and strain of our suspension system increased.

Similar to the steps in the previous section, the structural sound intensity of a suspension system under different loads could be evaluated, as shown in Figure 12. It can be seen that there was a large degree of structural sound intensity near the rim edge and hub. With an increase of load, the structural sound intensity of suspension system increased.

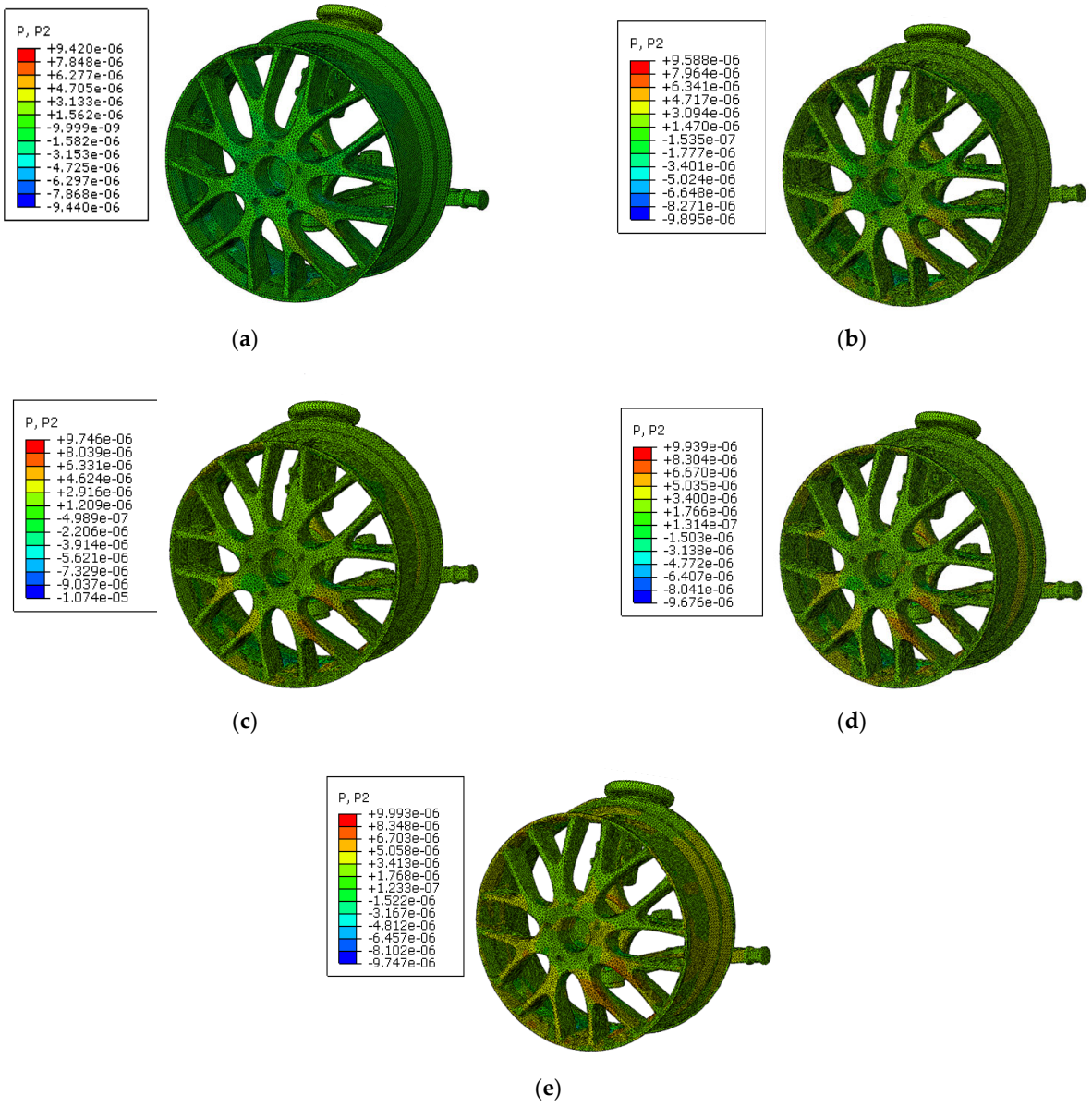


Figure 12. Power flow contour of a suspension system under different loads. (**a**) Power flow contour under 2500 N load. (**b**) Power flow contour under 3000 N load. (**c**) Power flow contour under 3500 N load. (**d**) Power flow contour under 4000 N load. (**e**) Power flow contour under 4500 N load.

For the suspension system under different loads, we calculated data such as the sum of the structural sound intensity and cross-sectional area at each point of the wheel input surface and three output surfaces. The power flow was obtained as shown in Table 5.

Table 5. Finite element calculation results of total power flow of input and three output sections.

Load Condition		Sum of Structural Sound Intensity (10^{-3} W/mm^2)	Number of Points	Cross Sectional Area (mm^2)	Power Flow of Cross Section (10^{-3} W)
2500 N	Input	2.831×10^{-2}	15,064	81,367	1.529×10^{-1}
	Output	2.793×10^{-4}	2652	11,180	1.177×10^{-3}
3000 N	Input	2.867×10^{-2}	15,064	81,367	1.549×10^{-1}
	Output	2.627×10^{-4}	2652	11,180	1.107×10^{-3}
3500 N	Input	2.848×10^{-2}	15,064	81,367	1.538×10^{-1}
	Output	2.503×10^{-4}	2652	11,180	1.055×10^{-3}
4000 N	Input	2.897×10^{-2}	15,064	81,367	1.565×10^{-1}
	Output	2.402×10^{-4}	2652	11,180	1.013×10^{-3}
4500 N	Input	2.975×10^{-2}	15,064	81,367	1.607×10^{-1}
	Output	2.290×10^{-4}	2652	11,180	9.652×10^{-4}

It can be seen from Table 5 that the total power flow of the three output surfaces of the suspension system under different loads was quite different, and different loads had obvious influences on the transmission of power flow. Additionally, the output power flow of the suspension system decreased slightly with an increase in load. It was this increase in load that led to an increase of input energy. In the process of energy transmission, damping consumes a great deal of energy, but the output energy is lower.

Based on the sound pressure amplitude distribution of the tire cavity resonance noise under different inflation pressure conditions under a load of 3500 N and at a speed of 50 km/h, as shown in Table 4, the power flow results of the input surface and three output surfaces of the suspension system were calculated, as shown in Table 6.

Table 6. Simulation results of sum power flow of input and three output sections.

Inflation Pressure Condition		Sum of Structural Sound Intensity (10^{-3} W/mm^2)	Number of Points	Cross Sectional Area (mm^2)	Power Flow of Cross Section (10^{-3} W)
0.16 MPa	Input	2.849×10^{-2}	15,064	81,367	1.539×10^{-1}
	Output	2.603×10^{-4}	2652	11,180	1.097×10^{-3}
0.19 MPa	Input	2.830×10^{-2}	15,064	81,367	1.529×10^{-1}
	Output	2.648×10^{-4}	2652	11,180	1.116×10^{-3}
0.22 MPa	Input	2.811×10^{-2}	15,064	81,367	1.518×10^{-1}
	Output	2.702×10^{-4}	2652	11,180	1.139×10^{-3}
0.25 MPa	Input	2.821×10^{-2}	15,064	81,367	1.523×10^{-1}
	Output	2.662×10^{-4}	2652	11,180	1.122×10^{-3}
0.28 MPa	Input	2.836×10^{-2}	15,064	81,367	1.532×10^{-1}
	Output	2.615×10^{-4}	2652	11,180	1.102×10^{-3}

From Table 6, it can be seen that the difference of the total power flow of the three output surfaces of the suspension system under different inflation pressures was small. Additionally, the influence of different inflation pressures on the transmission of power flow was not significant. The inflation pressure was 0.22 MPa, and the output power flow

of the suspension system was the largest. Under the other four inflation pressures, the output power flow of the suspension system was relatively low.

Based on the sound pressure amplitude distribution of the tire cavity resonance noise under different speed conditions with 0.22 MPa inflation pressure and 3000 N load, the power flow results of the input surface and three output surfaces of the suspension system were calculated, as shown in Table 7.

Table 7. Simulation results of total power flow of input and three output sections.

Speed Condition		Sum of Structural Sound Intensity (10^{-3} W/mm^2)	Number of Points	Cross Sectional Area (mm^2)	Power Flow of Cross Section (10^{-3} W)
20 km/h	Input	2.566×10^{-2}	15,064	81,367	1.386×10^{-1}
	Output	2.958×10^{-4}	2652	11,180	1.247×10^{-3}
30 km/h	Input	2.635×10^{-2}	15,064	81,367	1.423×10^{-1}
	Output	2.894×10^{-4}	2652	11,180	1.220×10^{-3}
40 km/h	Input	2.701×10^{-2}	15,064	81,367	1.459×10^{-1}
	Output	2.815×10^{-4}	2652	11,180	1.187×10^{-3}
50 km/h	Input	2.782×10^{-2}	15,064	81,367	1.503×10^{-1}
	Output	2.722×10^{-4}	2652	11,180	1.148×10^{-3}
60 km/h	Input	2.867×10^{-2}	15,064	81,367	1.549×10^{-1}
	Output	2.627×10^{-4}	2652	11,180	1.107×10^{-3}

From Table 7, it can be seen that for the suspension system at different speeds, the total power flow of the three output surfaces was quite different. Additionally, different speeds had an obvious influence on the transmission of power flow. As the speed increased, the output power flow of the suspension system decreased slightly.

5. Conclusions

In this research, the finite element model of a McPherson suspension system was established and the correctness of this model was verified by modal analysis. Finally, the power flow method was used to research the propagation characteristics of TCRN in the suspension system, and the propagation characteristics of TCRN at different running speeds, inflation pressures, and loads were obtained. The related conclusions are as follows:

(1) During the transmission of tire cavity resonance noise in a Y-spoke aluminum alloy wheel and suspension system, the power flow output by the lower arm front bushing is the largest and the power flow output by the rear bushing is the smallest.

(2) The areas in the suspension system with high stress are located at the steering knuckle, lower swing arm, and shock absorber. With an increase in load, the stress and strain of a suspension system increase, and the structural sound intensity of the suspension system increases.

(3) The output power flow of a suspension system decreases slightly with an increase in load. In our study, the output power flow of the suspension system was the largest when the inflation pressure was 0.22 MPa; the output power flow was relatively low under the other four inflation pressures. As the speed increased, the output power flow of the suspension system decreased slightly.

Studying the propagation characteristics of tire cavity resonance noise in suspension systems can provide a basis for the design of wheels and suspension systems which could suppress the propagation of tire cavity resonance noise.

Author Contributions: Conceptualization, X.L. and X.H.; methodology, X.H.; software, X.H.; validation, X.L., X.H. and Y.S.; investigation, T.H.; data curation, X.H.; writing—original draft preparation, X.H.; writing—review and editing, X.L.; visualization, X.H.; supervision, X.L. All authors have read and agreed to the published version of the manuscript.

Funding: This research was funded by the Natural Science Foundation of China grant number 51675021.

Institutional Review Board Statement: Not applicable.

Informed Consent Statement: Not applicable.

Data Availability Statement: The data presented in this study are available on request from the corresponding author. The data are not publicly available due to the requirements of the university.

Conflicts of Interest: The authors declare no conflict of interest.

References

1. Arpanahi, R.A.; Eskandari, A.; Mohammadi, B.; Hashemi, S.H. Study on the effect of viscosity and fluid flow on buckling behavior of nanoplate with surface energy. *Results Eng.* **2023**, *18*, 101078. [CrossRef]
2. Arpanahi, R.A.; Hashemi, K.H.; Mohammadi, B.; Hashemi, S.H. Investigation of the vibration behavior of nano piezoelectric rod using surface effects and non-local elasticity theory. *Eng. Res. Express* **2023**, *5*, 035029. [CrossRef]
3. Arpanahi, R.A.; Mohammadi, B.; Ahmadian, M.T.; Hashemi, S.H. Study on the buckling behavior of nonlocal nanoplate submerged in viscous moving fluid. *Int. J. Dyn. Control.* **2023**, *11*, 2820–2830. [CrossRef]
4. Deng, S.T. Investigation on Vibration Energy Transfer Characteristics of Beam Structures in Ladder Frame Chassis. Master's Thesis, Hunan University, Changsha, China, 2021.
5. Dzierzek, S. Experiment-based modeling of cylindrical rubber bushings for the simulation of wheel suspension dynamic behavior. *SAE Trans.* **2000**, *109*, 78–85.
6. Feng, B. Methods for Modeling and Parameters Identification of Rubber Bushing. Master's Thesis, Jilin University, Changchun, China, 2015.
7. Gavrić, L.; Pavić, G. A finite element method for computation of structural intensity by the normal mode approach. *J. Sound Vib.* **1993**, *164*, 29–43. [CrossRef]
8. Hu, X.; Liu, X.; Wan, X.; Shan, Y.; Yi, J. Experimental analysis of sound field in the tire cavity arising from the acoustic cavity resonance. *Appl. Acoust.* **2019**, *161*, 107172. [CrossRef]
9. Hu, X.; Liu, X. Research on Tire Cavity Resonance Mechanism and Its Noise Characteristics. Doctoral Thesis, Beihang University, Beijing, China, 2021.
10. Kim, G.J.; Holland, K.R.; Lalor, N. Identification of the airborne component of tyre-induced vehicle interior noise. *Appl. Acoust.* **1997**, *51*, 141–156. [CrossRef]
11. Lyon, R.H.; Maidanik, G. Power flow between linearly coupled oscillators. *J. Acoust. Soc. Am.* **1962**, *34*, 623–639. [CrossRef]
12. Li, Z. Analysis of the Performance of Rear Drive Axle Suspension with Rubber Bushing. Master's Thesis, Nanjing University of Aeronautics and Astronautics, Nanjing, China, 2016.
13. Li, X. Research on Fusion Control Strategy of Semi-Active Seat Suspension System for Both Vibration and Shock Mitigation. Master's Thesis, Hefei University of Technology, Hefei, China, 2021.
14. Li, X.P.; Li, F.J.; Yang, L.X.; Liu, X.L. Optimization design and dynamics analysis of vehicle suspension system. *J. Northeast. Univ. (Nat. Sci.)* **2020**, *41*, 1097–1102.
15. Mohamed, Z.; Wang, X.; Jazar, R. A survey of wheel tyre cavity resonance noise. *Int. J. Veh. Noise Vib.* **2013**, *9*, 276–293. [CrossRef]
16. Mohamed, Z.; Egab, L.; Wang, X. Tyre cavity coupling resonance and countermeasures. *Appl. Mech. Mater.* **2014**, *471*, 3–8. [CrossRef]
17. Mohamed, Z. A Study of Tyre Cavity Resonance Noise Mechanism and Countermeasures Using Vibroacoustic Analysis. Doctoral Thesis, RMIT University, Melbourne, VIC, Australia, 2014.
18. Pinnington, R.J.; White, R.G. Power flow through machine isolators to resonant and non-resonant beams. *J. Sound Vib.* **1981**, *75*, 179–197. [CrossRef]
19. Qiu, S. Simulation and Analysis of Vehicle Ride Comfort Affected by Suspension Rubber Bushing. Master's Thesis, Beijing Institute of Technology, Beijing, China, 2016.
20. Stephen, A.H.; Richard, P.S. Predictions of structural intensity fields using solid finite elements. *Noise Control Eng. J.* **1999**, *47*, 209–217.
21. Wu, Y.Y. Analysis and Optimization Design of Vibration Characteristics of Electric Vehicle Powertrain Mounting System. Master's Thesis, Shandong University, Jinan, China, 2020.

22. Weisser, T.; Foltête, E.; Bouhaddi, N.; Gonidou, L.O. A power flow mode approach dedicated to structural interface dynamic characterization. *J. Sound Vib.* **2015**, *334*, 202–218. [CrossRef]
23. Zhao, P. Analysis and Optimization of the Rubber Bushing Influence on the K&C Characteristic of Suspension. Master's Thesis, Chongqing University of Technology, Chongqing, China, 2013.

Disclaimer/Publisher's Note: The statements, opinions and data contained in all publications are solely those of the individual author(s) and contributor(s) and not of MDPI and/or the editor(s). MDPI and/or the editor(s) disclaim responsibility for any injury to people or property resulting from any ideas, methods, instructions or products referred to in the content.